7

# Surface-Enhanced Raman Scattering Sensors based on Hybrid Nanoparticles

Rafael Contreras-Cáceres, Benjamín Sierra-Martín and Antonio Fernández-Barbero
*Applied Physics Department, University of Almería*
*Spain*

## 1. Introduction

Surface-enhanced Raman scattering (SERS) is a powerful vibrational spectroscopic technique that allows ultra-sensitive chemical or biochemical analysis (Kneipp, Kneipp et al. 1999). It works by increasing the Raman signal of analyte molecules located nearby the surface of metallic nanostructures that can undergo localized surface plasmon resonance. Among these nanostructures, gold and silver nanoparticles are the dominant substrates, for both experimental and theoretical perspectives (Kneipp, Wang et al. 1997; Nie and Emery 1997), since they can support plasmon resonance properties able to increase the Raman signal up to 14 or 15 orders of magnitude, high enough to detect single molecules (Nie and Emery 1997; Qian and Nie 2008). Since the first report concerning the enhanced Raman signal of pyridine molecules adsorbed on a roughened silver electrode (Fleischm, Hendra et al. 1974), considerable efforts have been made in understanding the SERS mechanisms (Schatz 1984; Campion and Kambhampati 1998). Nowadays, analytical applications have centred the attention, and research is devoted to optimize the specific conditions for detecting each particular analyte (Porter, Lipert et al. 2008). Interestingly, the enhancement factor is found to depend on the different affinity of the functional groups in the analyte toward gold or silver surfaces because it is the affinity which determines the analyte retention (Pearson 1963; Pearson 1966). To improve the surface-analyte interaction, various approaches have been developed, including the functionalization of nanoparticle surface (Guerrini, Garcia-Ramos et al. 2006; Guerrini, Garcia-Ramos et al. 2008); however, a problem inherent to this alternative is that usually the assembled molecules provide strong SERS signals that overlap and screen those corresponding to the analyte. Another alternative relies on controlling the surface charge of the nanoparticles to promote the electrostatic attraction of the analyte onto the particle surface (Alvarez-Puebla, Arceo et al. 2005; Aroca, Alvarez-Puebla et al. 2005). This approach has been reported to consistently enhances the signal for acids and amines, but it hardly helps in the case of alcohols, ethers, and other oxygen containing groups, as well as for non-functionalized molecules. Thereby, there is a clear need for development of new nanocomposites, based on noble-metals, containing a sensitive material that enables the physical trapping of a wide variety of analyte molecules.
Herein we present the synthesis and applications of novel core-shell nanocomposites comprising Au and Au-Ag bimetallic cores, with spherical or rod-shaped morphology,

coated with thermally responsive poly-(N-isopropylacrylamide) (pNIPAM) microgel (Contreras-Caceres, Sanchez-Iglesias et al. 2008). In these systems, whereas the metallic core provides the necessary enhancing properties, the pNIPAM shell, that can swell or collapse as a function of temperature, is used to trap the analyte molecules and get them sufficiently close to the core. These materials present unique optical properties as a consequence of the thermally responsive surface plasmon resonance, which can be ultimately exploited for SERS analysis. Although similar systems have been proposed for applications in catalysis (Lu, Mei et al. 2006), temperature or pH sensing (Kim and Lee 2004), or light-responsive materials (Gorelikov, Field et al. 2004), we report here that the hybrid nanoparticles can function as general sensors for detecting different types of analytes. Apart from the SERS enhancement, these nanocomposites can also be used to modulate the fluorescence intensity of adsorbed chromophores as a function of temperature. It is important to note, that the pNIPAM shell not only enhances the colloidal stability of the system in aqueous solutions, but additionally prevents electromagnetic coupling between metal particles, thus providing highly reproducible SERS signal and intensity, which is crucial for quantitative applications. Through a rational choice of model analytes, we report the applications of these thermoresponsive hybrid materials for Surface Enhanced Raman Scattering and Fluorescence (SERS and SEF, respectively). The nanocomposites are first tested using 1-naphthalenethiol (1NAT) as a model analyte with large affinity for gold, and consecutively against a common dye, Nile Blue A (NBA), whose affinity for gold is lower than of 1NAT. In addition, we present the SERS analysis of 1-napthol, a substance that had remained elusive for SERS since it does not easily adsorb onto conventional silver or gold surfaces and whose detection is decisive because is considered a relevant biomarker (Hansen, Omland et al. 1994; Sun, Shen et al. 2008) and also causes genotoxicity under chronic exposure to humans (Kozumbo, Agarwal et al. 1992; Grancharov, Engelberg et al. 2001). To conclude the report, the SERS efficiency of the different hybrid nanocomposites is compared for a couple of analytes. The wide range of systems investigated, lead us to establish the effect of parameters, such as particle morphology or core composition, on the detection capabilities. Interestingly, sensors based on Au-Ag core coated by the pNIPAM shell are found to provide much higher SERS intensities than their Au-pNIPAM counterparts, not only in the case of spheres but particularly for nanorods.

## 2. Plasmon resonance and surface-enhanced Raman scattering

Plasmons are quantized collective oscillations of the free electron gas density that occurs between any two materials whose dielectric function changes sign across the interface, for instance metal-dielectric interfaces (Barnes, Dereux et al. 2003). Surface plasmons are those confined to surfaces; they can strongly couple with photons resulting in surface polaritons, which are considered quasi-particles that propagate along the metal surface until its energy decays via absorption into the metal or radiation into the free-space (Zayats, Smolyaninov et al. 2005). Light or electric fields can excite those plasmons, then resulting in surface and localized surface plasmon resonance (SPR and LSPR) in the case of planar and nanometric-sized metallic structures, respectively (Mulvaney 1996). Plasmon oscillation is resonant with the light at a particular frequency. The electric field intensity, the scattering and the adsorption cross-sections are then enhanced. Materials exhibiting surface plasmon properties are used to maximize surface sensitive spectroscopic techniques, such as Raman scattering or fluorescence (Hutter and Fendler 2004). The resonance frequency strongly

depends on the size and shape of the metal nanoparticles, as well as, on the metal complex dielectric function and surrounding medium. Noble metals such as copper, silver, and gold exhibit strong visible-light plasmon resonance, whereas other transition metals show only a broad and poorly resolved absorption band in the ultraviolet region (Link and El-Sayed 1999). To understand the optical properties of these metals, it is not only necessary to account for the effect of free-electrons, responsible for plasmon resonance, but also for the interband transitions (Wang, Tam et al. 2005). For instance, copper nanoparticles have strong interband transitions which overlap with the plasmon resonance energies, then leading to a damping effect that minimizes its optical response. Contrarily, in case of gold and silver nanoparticles, both effects are well separated in the spectrum. Therefore, electrons of the conduction band can move freely, showing higher polarizability. This fact, in turn shifts the plasmon resonance to lower frequencies with sharp bandwidth. Since copper is also easily oxidized, gold and silver nanoparticles are more attractive for optics-based applications, specifically silver since it has by far the strongest plasmon resonance. In this case, the higher plasmon energy respect to that of the interband transition results in minimum damping effect (Johnson and Christy 1972). Localized plasmon resonance is responsible for the intense colour of metal nanoparticle dispersions (Bohren and Huffman 1983); the resultant absorption bands are exploited for technical applications like photovoltaic cells (Pillai, Catchpole et al. 2007). In other applications, it is desirable to tune the plasmon resonance depending on the availability of a suitable laser to enhance the optical properties (Willets and Van Duyne 2007; Homola 2008). Although increasing spherical-nanoparticle size causes red-shift due to electromagnetic retardation, the range of frequencies is quite limited (Jain, Huang et al. 2008). Alternatively, LSPR can be tuned by changing the particle morphology, from spherical to rod-shaped. Metal nanorods show typically two resonance peaks corresponding to plasmon oscillations along the short and long axis (Murphy, San et al. 2005). As the aspect ratio, defined as the length-to-width ratio, is increased, the LSPR associated to the long axis is red-shift from visible to near infrared region. The same effect can be achieved by coating a solid sphere with metallic shells (Oldenburg, Averitt et al. 1998); the LSPR frequency decreases as the ratio shell thickness-core size reduces, being the relation almost exponential regardless of the core and shell composition (Jain and El-Sayed 2007).

Surface-enhanced Raman scattering is based on the enhancement of Raman signal induced by plasmonic metal surfaces on nearby molecules (Otto, Mrozek et al. 1992). The extent of enhancement depends on the shape and size of the metal nanoparticles, as these factors influence the ratio of absorption and scattering events (Bao, Mahurin et al. 2003). Large particles allow multipole excitation, which are nonradiative modes; since only dipolar transitions contribute to Raman scattering, the overall efficiency of the enhancement is then reduced. On the other side, too small particles lose their electrical conductance and cannot enhance the field. When the size approaches a few atoms, the definition of plasmon, which involves a large collection of electrons to oscillate together, does not hold (Moskovits 2006). The enhancement factor is maximum for nano-structured metals (10-100 nm) (Tian, Ren et al. 2002), being thus excellent materials for SERS. The exact mechanism accounting for the enhancement effect is still a matter of debate (Qian and Nie 2008). Although several models have been proposed in the literature, nowadays, two mechanisms are accepted (Campion and Kambhampati 1998): electromagnetic and chemical. The first one relies on the excitation of localized surface plasmon on metal surfaces, whereas the second one proposes changes of the molecule electronic structure (Vo-Dinh 1998). The chemical enhancement only applies in

specific cases that cannot be explained by the electromagnetic mechanism. For instance, the SERS signal for molecules with almost the same polarizability differs in a factor of 200, even though the electromagnetic model establishes a non selective amplification. Moreover, the transition HOMO-LUMO for many molecules (between the highest occupied and the lowest unoccupied molecular orbital) can occurs at about half the energy in SERS experiments. The formation of charge transfer complexes or chemical bounds between the metal surface and the analyte (necessary in the chemical model) can explain the observed enhancement (Lombardi, Birke et al. 1986). The chemical mechanism is short ranged (0.1-0.5 nm) and strongly dependent on the geometry of bonding and on the molecule energy level. Anyhow, the contribution of this mechanism to SERS is relatively small; its enhancement is estimated to be a factor $10^1$-$10^3$. Instead, the electromagnetic mechanism is the dominant contribution in SERS. It accounts for more situations, even for molecules not adsorbed on the surface (Xu, Aizpurua et al. 2000). According to the electromagnetic model (Fig. 1), the incident electromagnetic field, $E_i$, excites the surface plasmons and induces oscillating dipoles given by $\mu(t) = \propto E_i(t)$, being $\propto$ the polarizability tensor (Stevenson and Vo-Dinh 1996). The plasmon oscillations must be perpendicular to the surface, otherwise scattering does not occurs (Smith and Dent 2005 ). The induced polarization generates large local fields on the particle; it magnifies the incident field, thus increasing the Raman signal . On a second step, the emitted Raman field, $E_R$, can also polarize the metal particle, which thereby acts as an antenna to further intensify the Raman signal. The Raman intensity is proportional to the square field . As a result of the first process, the intensity enhances $(E_i+E_{i,s})^2$ , whereas for the second step, it increases $(E_R+E_{R,s})^2$ (Schlucker 2009). The frequency-shift between the incident light and the Raman signal

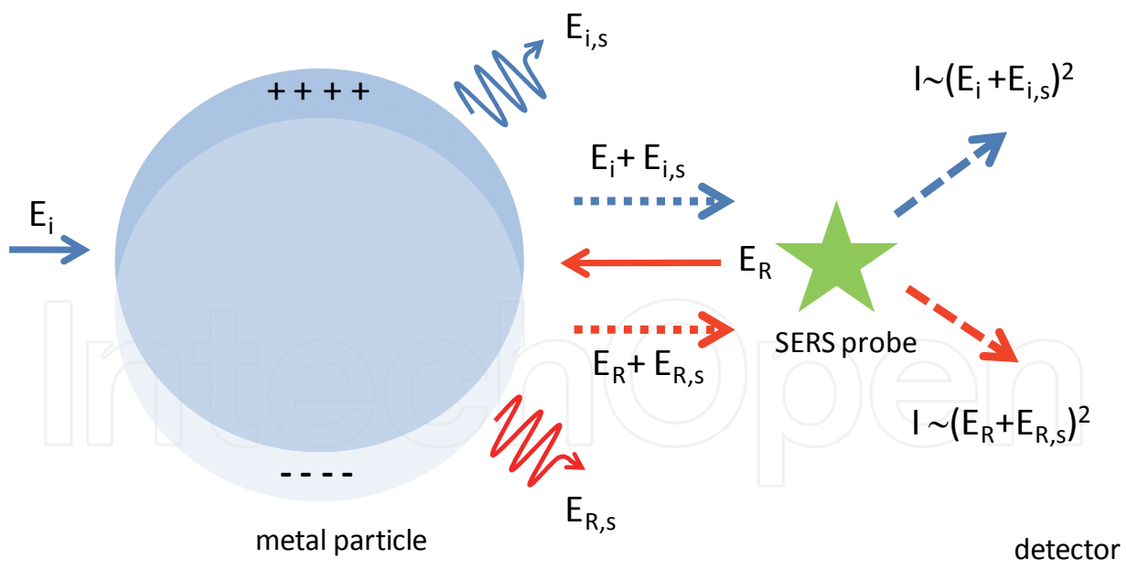


Fig. 1. Schematic representation of the electromagnetic enhancement mechanism in SERS. There are two processes: i) (blue) the incident field, $E_i$, is enhanced due to the addition of the scattered field, $E_{i,s}$. It arises from the particle polarization, yielding the field $E_i + E_{i,s}$ and exciting Raman modes on the probe molecule; ii) (red) the emitted Raman field, $E_R$, is also enhanced through the same mechanism. The improved field $E_R + E_{R,s}$ further enhances the Raman intensity, I. Raman signal is enhanced $E^2$ in each process.

determines the extent of enhancement. For small shifts, both fields can be nearly resonant with the surface plasmon, then establishing a total enhancement of $E^4$. Gold and silver are mostly used for SERS because their plasmon resonance frequencies fall within the wavelength range used to excite Raman modes, namely visible and near-infrared regions of the spectrum. SERS enhancement also depends on the distance between the nanoparticle centre and the target molecule, R; it falls off as ~ $(r/R)^{12}$, where r is the particle radius (Stiles, Dieringer et al. 2008). This expression indicates that molecule is not required to be just in contact with the surface. Especially useful are those nanostructures capable of controlling R, in order to tune the Raman enhancement in an accurate way (Alvarez-Puebla, Contreras-Caceres et al. 2009).

## 3. Hybrid nanoparticles: Synthesis and optical properties

### 3.1 Au-pNIPAM core-shell nanoparticles

Spherical gold nanoparticles are typically prepared in a wide range of size from aqueous solutions of cationic surfactant cetyltrimethylammonium bromide (CTAB) using a seeded growth method, in which ionic precursors are reduced by ascorbic acid in the presence of preformed gold seeds (Jana, Gearheart et al. 2001; Rodriguez-Fernandez, Perez-Juste et al. 2006). The reducing agent role can also be played by other reducing acids, such as salicylic acid, producing similar effect; salicylic acid reduces $Au^{III}$-CTAB complexes to $Au^{I}$-CTAB, although the final reduction into $Au^0$ only happens on the catalytic gold surface (Okamoto and Hachisu 1977). In this chapter we review a novel procedure based on butenoic acid as reducing agent (Contreras-Caceres, Pastoriza-Santos et al.); it is supported on the reducing capability of the vinyl group, present in butenoic acid, toward $HAuCl_4$, used as gold salt precursor (Yavuz, Li et al. 2009). Indeed, the use of butenoic acid is particularly interesting because it provides the particles with vinyl functionality, then making this method useful for direct pNIPAM polymerization on the particle surface and their subsequent encapsulation, avoiding any surface functionalization step. Butenoic acid replaces CTAB molecules from the particle-solvent interface and absorbs on it, thereby promoting polymerization of pNIPAM shells. This may be used on a wide set of preformed particles with interesting morphologies, including nanorods. The polymer shell porosity allows subsequent reduction of metal atoms above the core; this is used as strategy for overgrowing the gold cores encapsulated into pNIPAM, with both spherical and rod-shaped morphologies.

**Au-sphere(64nm)@pNIPAM particles**. Preparation is based on a seeded growth method using 15 nm Au seed particles, previously prepared under citrate reduction. Briefly, 35 mL of this particle suspension is added to a CTAB aqueous solution (15 mL, 0.03 M). A volume of 4.5 mL of the seed solution is then added to a growth solution prepared under gentle magnetic stirring at 70ºC, with 800 µL of butenoic acid and 50 mL of aqueous solution containing $HAuCl_4$ (1 mM) and CTAB (15 mM). After 10 minutes, the excess of butenoic acid and CTAB is removed by centrifugation (4500 rpm, 30 min). Next, the pellet is re-dispersed into CTAB (50 mL, 4 mM), centrifuged (4500 rpm, 40 min), and the precipitated re-dispersed again into water (10 mL). The resultant dispersion is heated at 70ºC under $N_2$ flow while the monomers, NIPAM (0.1698 g) and N,N'-methylenebisacrylamide, BIS, (0.0234 g) are added under magnetic stirring. After 15 min, the nitrogen flow is stopped and the polymerization initiated with 2,2'-azobis(2-methylpropionamidine) dihydrochloride, AAPH, (100 µL, 0.1 M). The reaction is extended for 2 h and then cool down to room

temperature under stirring. The sample is finally diluted into water (50 mL), centrifuged (4500 rpm, 30 min) and re-dispersed into water (5 fold). The gold core size measured by TEM is 63.9 ± 5.9 nm.

**Au-sphere(103nm)@pNIPAM particles.** The particles are prepared by growing the gold cores of the particles previously described. Ascorbic acid, AA, (180 μL, 0.1M) is added, under magnetic stirring, to 10 mL of aqueous solution containing Au-spheres(64nm)@pNIPAM (0.25 mM), CTAB (0.1 M) and $HAuCl_4$ (0.9 mM). After 30 min, the growth process is concluded, yielding particles with 103.0 ± 8.4 nm average core size .

**Au-nanorod@pNIPAM particles.** A gold nanorod suspension is first synthesized following the seed-mediated method reported here (Liu and Guyot-Sionnest 2005). (70.0 ± 7.2) nm long x (17.6 ± 3.1) nm wide gold particles are obtained, which gives aspect ratio AR=4.1. The dispersion (100 mL) is centrifuged (7000 rpm, 1 h) to remove the excess of CTAB and re-dispersed into water (100 mL). Next, butenoic acid (300 μL) is added to this solution at 70ºC. After 1 hour, the dispersion is again centrifuged (6000 rpm, 1 h) to remove any excess of butenoic acid and re-dispersed into water (10 mL). Encapsulation with pNIPAM is performed following the method described for Au(64nm)@pNIPAM particles, differing only on the amount of monomer, NIPAM (0.1924 g) and BIS (0.0265). Once the polymerization is completed, the dispersion is diluted into water (50 mL), centrifuged (5500 rpm, 1 h) and re-dispersed into water (5 fold).

**Au-nanorod@Au@pNIPAM particles.** The growth of Au-nanorod@pNIPAM particles is carried out as previously described for Au-sphere(103nm)@pNIPAM, but using 0.8 mM $HAuCl_4$ and 160 μL of 0.1 M AA. The final core size is (82.1 ± 7.9) nm x (21.6 ± 2.6) nm, with aspect ratio AR= 3.6. The synthesis using butenoic acid leads to extremely efficient coverage of the gold core (Fig. 2a). TEM image shows that all the particles are perfectly encapsulated, confirming that the presence of vinyl groups on the particle periphery promotes uniform pNIPAM polymerization on the particle surfaces, as previously observed for gold and silica particles (Zha, Zhang et al. 2002; Guerrini, Garcia-Ramos et al. 2006; Karg, Pastoriza-Santos et al. 2006; Guerrini, Garcia-Ramos et al. 2008). The morphology is clearly visible from TEM images. The intense core black-color is due to the higher electron density respect to the organic shell. Further information about the core-shell structure is obtained by atomic force microscopy (AFM), as illustrated by the inset on Fig. 2a. The image is taken in tapping mode on a dried sample, previously prepared on silicon wafer; during dehydration, pNIPAM shell spreads while the gold core stands out from the polymer coverage. The size and plasmonic response of the core-shell nanocomposites may be tuned with temperature in a reversible way. Fig. 2b shows the UV/Vis-NIR spectra, obtained in the range 16ºC (swollen shell) and 56ºC (collapsed shell). As temperature increases, the plasmon band high increases and red-shifts. Both effects are associated to the increase of the microgel shell refractive index during collapse, with enhancement of the Rayleigh scattering (Kozumbo, Agarwal et al. 1992; Grancharov, Engelberg et al. 2001; Karg, Pastoriza-Santos et al. 2007). The localized surface plasmon resonance (LSPR) shifts the peak position with temperature, inversely to the size variation, as shown in Fig. 2c. The pNIPAM shell lower critical solution temperature (LCST) is similar to that reported for pure microgel (Kratz, Hellweg et al. 2001), while the LSPR bands are consistently red-shifted as microgel shell collapses due to the increase on the refractive index around the metal core. As expected, the LSPR position is nicely correlated to the hydrodynamic diameter.

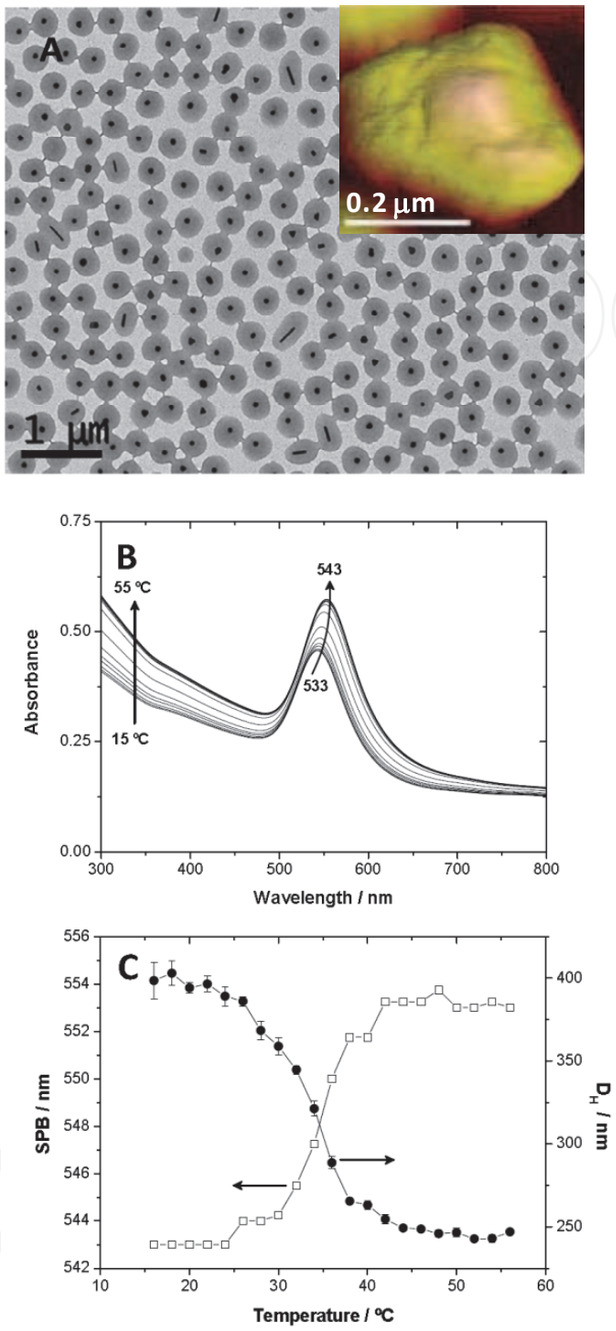


Fig. 2. Characterization of the system Au-sphere(64nm)@pNIPAM. (A) TEM image (microscope JEOL JEM 1010, operating at an acceleration voltage of 100 kV). The inset corresponds to a tapping mode AFM image (Veeco Nanoscope, spring constant $k$ = 20-80 $Nm^{-1}$; (B) UV-vis spectra at different temperatures (Cary 5000 spectrophotometer); (C) Localized surface plasmon band position (SPB) (squares) and hydrodynamic diameter (circles) temperature dependence. Particle size is measured by dynamic light scattering (Malvern Zetasizer Nano S) using cumulant-type analysis. Reprinted with permission from (Contreras-Caceres, Pastoriza-Santos et al.), Copyright (2010) by Wiley-VSC Verlag GmbH & Co. KGaA

### 3.2 Bimetallic-pNIPAM core-shell nanoparticles

An advantage of using core-shell gold-pNIPAM particles is the excellent colloidal stability and porosity provided by the shell, especially when the polymer is swollen. They can behave as microreactors where chemical reactions can be performed. In addition, they allow further reduction of metals on the gold core, addressed not only to control the core size (Contreras-Caceres, Pacifico et al. 2009) but also the core nature (Sanchez-Iglesias, Grzelczak et al. 2009). Inasmuch that silver is significantly much efficient for SERS than gold, it is important to incorporate this metal to the nanocomposites. Direct synthesis of size and shape-controlled silver nanoparticles is complicated. An alternative method is to grow silver shells on preformed gold nanoparticles with both spherical or rod-shaped core. The resultant nanocomposites display optical properties close to those of pure silver (Cho, Camargo et al.). The method simply involves the reduction of $AgNO_3$ using ascorbic acid in the presence of the corresponding particle as template.

**Au-sphere(64nm)@Ag@pNIPAM particles.** Preparation relies on the process for coating pure gold particles with silver (Yang, Lin et al. 2005). A dispersion of preformed Au-sphere(64 nm)@pNIPAM particles (10 mL, 0.25 mM) containing CTAB (50 mM) is set to pH=9.5 with glycine buffer. Next, $AgNO_3$ aqueous solution (655 µL, 15.2 mM) and ascorbic acid (450 µL, 0.1 M) is added. The reduction reaction is extended over 30 minutes, then rendering a bimetallic 100.3 ± 9.2 nm Au@Ag core size.

**Au-nanorod@Ag@pNIPAM particles.** The growth process is performed as previously described for Au-sphere(64nm)@Ag@pNIPAM, being the only difference the amount of $AgNO_3$ (540 µL, 14.83 mM) and ascorbic acid (360 µL, 0.1 M) aqueous solutions. The final core size for the bimetallic nanorods is (76.7 ± 7.7) nm long x (40.0 ± 5.1) nm wide, with aspect ratio AR=1.9. In previous works NaOH was used to increase the solution pH, leading to the nucleation of small Ag nanoparticles, and consequently to percentage reduction of core-shell particles (Rodriguez-Gonzalez, Burrows et al. 2005). However, for the present method using a glycine buffer, the reduction slows down (Pearson 1963; Pearson 1966), then avoiding the presence of small silver nuclei. This growing method is very efficient, not only for silver growing but also for gold. Fig. 3 (A and C) shows representative TEM images of particles with Au cores (spheres and rods, respectively), whereas Fig. 3 (B and D) illustrates those formed with silver shell. It is noticeable the intensity contrast existing between Au core and Ag shell; it arises from the electron scattering difference between both metals and clearly shows the uniform coating for both geometries. The overall dimensions for the particles, including the pNIPAM shell, are similar before and after the different core growth processes (Contreras-Caceres, Pastoriza-Santos et al.). The different nanocomposites are expected to have different optical properties. Fig. 3 shows pictures corresponding to the aqueous dispersions; it can be observed by simple visual inspection how color changes, indicating shifting of the localized surface plasmon peak.

The optical signatures for the different nanocomposites are recorded by UV-visible spectroscopy and summarized in Fig. 4. It is noticeable (Fig. 4A) that, whereas the growth of Au spherical cores, from 64 to 103 nm, leads to significant redshift due to retardation effects (Rodriguez-Fernandez, Perez-Juste et al. 2006), the coating with Ag (of almost the same thickness), remarkably results in blue-shift and formation of quadrupolar modes, in agreement with previous works (Rodriguez-Gonzalez, Burrows et al. 2005). In the case of rod-shaped cores growing with gold (Fig. 4B), there is no displacement of the localized

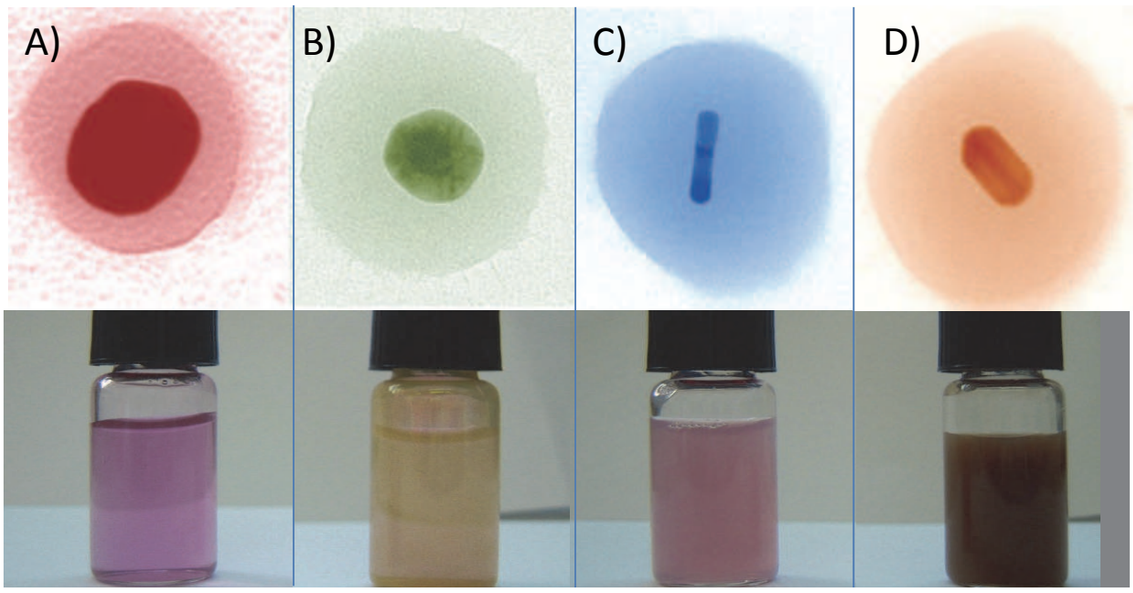


Fig. 3. (Up) Representative TEM images of hybrid nanoparticles with different morphologies; color is retouched to emphasize the core-shell structure. (Down) Pictures of their corresponding aqueous dispersions: (A) Au-sphere(103nm)@pNIPAM; (B) Au(64nm)@Ag(36nm)-sphere@pNIPAM; (C) Au-nanorod@pNIPAM (82.1nm x 21.6 nm); (D) Au-Ag-nanorod@pNIPAM (76.7 nm x 40.0 nm).

plasmon resonance, only the band intensity increases; this demonstrates that the growth process is uniform, with no significant change of the aspect ratio. For silver growth, a dramatic blue-shift of the longitudinal LSPR appears, not only due to the presence of silver on the surface, but also because the growth process occurs preferentially at the rod sides, in agreement with recent reports (Sanchez-Iglesias, Carbo-Argibay et al.). The core-grown nanocomposites preserve the original thermo-responsive properties of the original core-shell particles used as template. Not only the size can be tuned through temperature changes, but also the optical properties are greatly influenced. In general, there is a red-shift of LSPR band as temperature rises above the LCST of 32°C, as a consequence of the polymer shell collapse. The extent of this red-shift depends on the metal core size, shape, and composition. These three factors are known to dominate the LSPR sensitivity toward changes of the local refractive index (Chen, Kou et al. 2008; Sepulveda, Angelome et al. 2009). For instance, within the explored range of temperature, the LSPR shift for Au-sphere(64 nm)@pNIPAM particles is 10 nm, whereas for Au(64 nm)@Ag@pNIPAM increases up to 17 nm. The largest LSPR shift is recorded for Au-nanorod@pNIPAM, about 28 nm, due to the higher electromagnetic field concentration in rods, which in turn leads to a higher sensitivity for local refractive index changes (Chen, Kou et al. 2008).

## 4. Entrapping target molecules: Surface-enhanced Raman analysis.

Gold-pNIPAM core-shell particles used in this section are synthesized by a slightly different method, consisting of an initial growth of thin polystyrene (PS) on preformed gold nanoparticles (67 nm) coated with CTAB, followed by in situ polymerization of the pNIPAM shell (Contreras-Caceres, Sanchez-Iglesias et al. 2008). Particles with larger metal cores

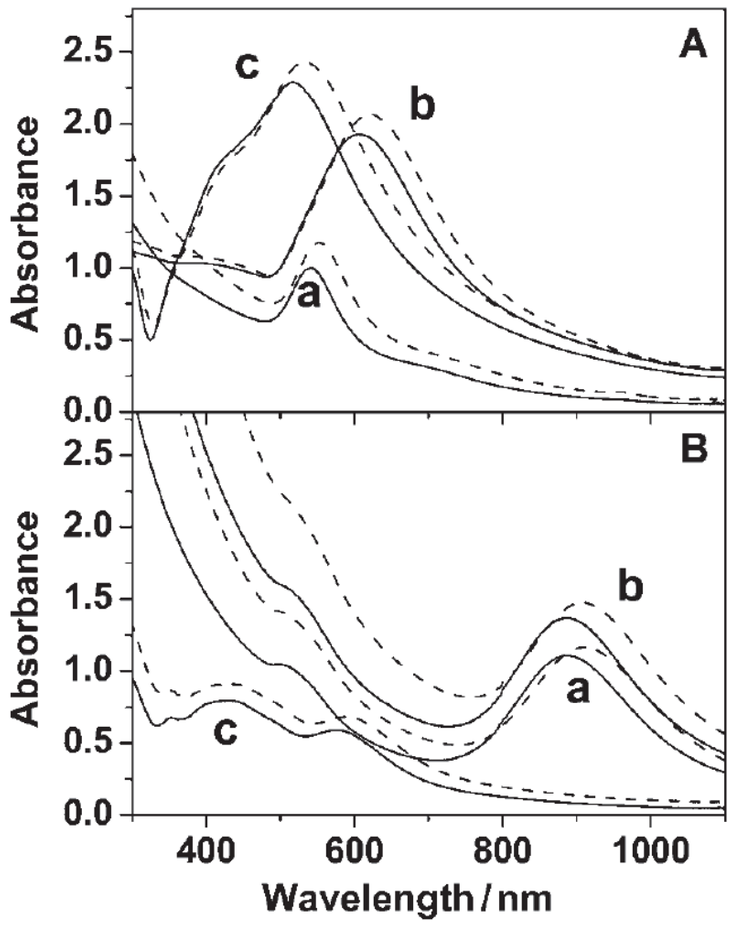


Fig. 4. UV-Vis-NIR spectra for aqueous dispersions of different core-shell metal@pNIPAM nanocomposites. Data are recorded at 22ºC (solid lines) and 44ºC (dash line), which corresponds to the swollen and collapsed shell states, respectively. (A) Sphere-coated particles: (a) Au-sphere (64 nm); (b) Au-sphere (103 nm); (c) Au@Ag core-shell sphere. (B) Rod-coated particles: (a) Au-nanorod; (b) Au@Au nanorod; (c) Au@Ag nanorod (10 time diluted to avoid scattering effects). Reprinted with permission from (Contreras-Caceres, Pastoriza-Santos et al.), Copyright (2010) by Wiley-VSC Verlag GmbH & Co. KGaA.

(116 nm) are prepared by seeded growth of the 67 nm coated gold cores through the addition of $HAuCl_4$ and ascorbic acid as reducing agent. The SERS spectrum of gold-polystyrene particles is shown in Fig. 5. The peaks correspond to ring C=C stretching (1615 $cm^{-1}$), $CH_2$ scissoring (1461 $cm^{-1}$), ring breathing (1012 $cm^{-1}$), and radial ring stretching mode (646 $cm^{-1}$), which are characteristic of polystyrene (Hong, Boerio et al. 1993). Interestingly, as particles polymerize with pNIPAM, the bands disappear showing an effective replacement of PS by pNIPAM, as also observed in Fig. 5, for both selected core sizes Au@pNIPAM (67 and 116 nm). Both spectra fit band to band, being represented by NH bending (1447 $cm^{-1}$), CN stretching (1210 $cm^{-1}$), $CH_3$ rocking (963 $cm^{-1}$), CH deformation (866 and 841 $cm^{-1}$), CC rocking (766 $cm^{-1}$), CNO bending (655 $cm^{-1}$), and CCO out-of-plane deformation (413 $cm^{-1}$). There is an important increase in intensity for large gold cores, as result of a considerable enhancement of the optical properties with increasing size, in agreement with previous

reports (Kelly, Coronado et al. 2003; Njoki, Lim et al. 2007). The overall SERS intensity (cross-section) obtained from pNIPAM is low, thus providing an excellent background for analytical applications. pNIPAM shell with thermoresponsive properties allows to entrap analyte molecules and approximate them to the metal core (when the polymer collapses) where Raman enhancement becomes apparent. In addition, shell prevents the electromagnetic metal particle coupling, with highly reproducible SERS signal and intensity. The fluorescence intensity of certain adsorbed chromophores can also be improved in such a way. We present here analytical applications based on SERS, SERRS and surface enhanced fluoresce (SEF), using gold-pNIPAM nanocomposites through a rational selection of analytes. All spectra are taken with a LabRam HR Raman equipment (Horiba-Jobin Yvon), following two kind of experiments. Firstly, the particle dispersion (1mL, $5x10^{-4}$ M in gold) together the analyte (10 µL, $10^{-5}$-$10^{-6}$ M) are stabilized at 4ºC for 2 h, time enough to reach thermodynamic equilibrium. Next, samples are excited with a 785 nm laser to collect the SERS spectra or with 633 nm laser for SFE and SERRS spectra. Thereafter, the samples are equilibrated at 60ºC for 2 h and again at 4ºC. After each equilibrium step, spectra are collected under the same experimental conditions. In a second experiment, equilibration steps are repeated, following the inverse temperature sequence, starting at 60ºC, cooling to 4ºC and heating back to 60ºC.

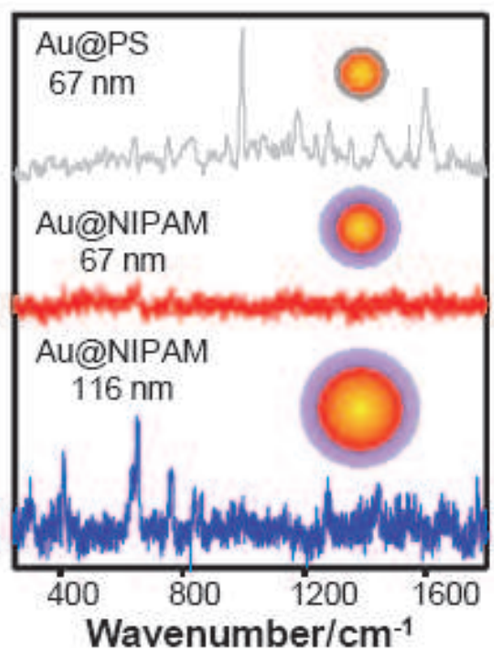


Fig. 5. (From top to bottom) SERS spectra of Au@PS particles, Au(67nm)@pNIPAM (obtained by coating Au@PS) and Au(116nm)@pNIPAM (after in situ growth of gold core). Acquisition time is 50 s. Reprinted with permission from (Contreras-Caceres, Sanchez-Iglesias et al. 2008), Copyright (2008) by Wiley-VSC Verlag GmbH & Co. KGaA.

### 4.1 Analyte with specific molecular interactions: 1-naphthalenethiol

Raman enhancing properties of Au-pNIPAM nanoparticles are initially tested using 1-naphthalenethiol (1NAT); this is a small molecule with large affinity for gold (through the

thiol group). It is considered a model analyte since it easily diffuses across the porous polymer shell. Moreover, its SERS spectrum is well established (Alvarez-Puebla, Dos Santos et al. 2004). As can be seen in Fig. 6a, the Raman spectrum is dominated by the ring stretching (1553, 1503, and 1368 $cm^{-1}$), CH bending (1197 $cm^{-1}$), ring breathing (968 and 822 $cm^{-1}$), ring deformation (792, 664, 539, and 517 $cm^{-1}$), and CS stretching (389 $cm^{-1}$). The intensity of the band at 1368 $cm^{-1}$, corresponding to the ring stretching, is plotted against temperature for both cooling-heating cycles.

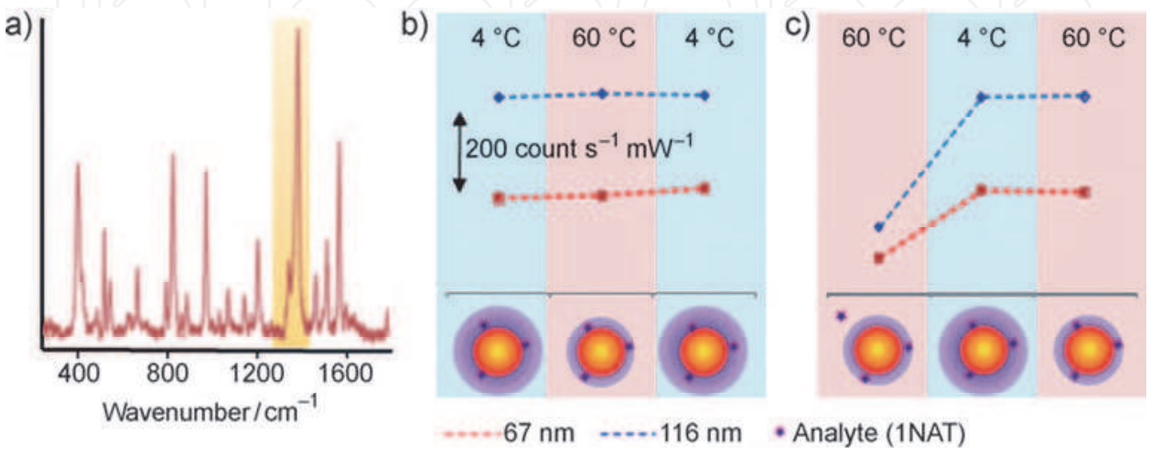


Fig. 6. (a) SERS spectrum of 1-naphtalenethiol dissolved in Au@pNIPAM particle dispersions. Excitation wavelength $\lambda_{ex}$= 785 nm. (b, c) Variation of the intensity of the band at 1368 $cm^{-1}$, ring stretching highlighted in yellow, as a function of gold-core size and temperature in two different cooling-heating cycles: (b) 4–60-4°C; and, (c) 60-4-60°C. Acquisition time is 2s for all experiments. Reprinted with permission from (Contreras-Caceres, Sanchez-Iglesias et al. 2008), Copyright (2008) by Wiley-VSC Verlag GmbH & Co. KGaA.

As the analyte is added to the nanoparticle dispersion at 4°C (Fig. 6b), pNIPAM shells swell, allowing the analyte to diffuse across the polymer to reach the gold-core surface, to which it readily chemisorbs. This results in a high SERS intensity, which remains high after gradually heating up to 60°C and cooling down back to 4°C. Instead, when 1NAT is added to the dispersion at 60°C, SERS signal is substantially lower (Fig. 6c). However, by cooling down temperature to 4°C, the signal surprisingly enhances up to intensities comparable to those of the previous cycle. Furthermore, the high signal remains stable during subsequent temperature changes. The results can be explained by considering the volume transition exhibited by the pNIPAM shell; above 32°C, shell changes from water-swollen to shrunken states, being the process totally reversible (Sierra-Martin, Choi et al. 2005). Thereby, as shells remain collapsed at 60°C, the diffusion of 1NAT through the network is hindered and the gold surface is not longer accessible, giving then low signal. Once the temperature cold down, the analyte adsorbs on the core and retains there regardless the gel swelling state. We suggest that 1NAT forms a covalent bound at the gold surface, which is consistent with the disappearance of the SH stretching peak in the SERS spectra and also with previous reports (Pearson 1963; Pearson 1966). It is interesting to note that the enhancement provided by the larger gold core (116 nm) is considerable higher, partly because of the better match between the excitation wavelength (785 nm) and the plasmon band (Creighton, Blatchford et al.

1979); as gold core size increases, the plasmon band shifts to higher wavelengths (Fig. 4). The enhancement factor calculated for this core-shell system is EF=5.16x10$^5$, a rather high value if we take into account that 1NAT does not present substantial charge-transfer enhancement (the so-called chemical effect) (McFarland, Young et al. 2005). The polymer shell prevents the electromagnetic coupling between particles, and hence the formation of hot spots. The enhancement factor is estimated by comparing the signal of the analyte with and without hybrid particles; it is given by equation $EF = (I_A V_A / I_B V_B) f$ (Alvarez-Puebla, Dos Santos et al. 2007), where $V_A$, $V_B$ are the probed volumes, $I_A$, $I_B$ the respective SERS intensities and f a correction factor that considers the concentration ratio of the target molecule in both experiments. We note that the forthcoming SERS experiments will be developed only with the Au(116nm)@pNIPAM system, provided that it induces the best Raman enhancement.

### 4.2 Non-interacting analytes

#### 4.2.1 Nile Blue A

A second demonstration of the potential applications of the Au-pNIPAM nanocomposite is developed for a common dye, Nile Blue A (NBA). This molecule is slightly larger than 1NAT. In addition, it contains an amine functional group which diminishes the affinity for gold surfaces respect to 1NAT (Pearson 1963; Pearson 1966). NBA molecules show different spectra, either SERS or SEF/SERRS, depending on the excitation wavelength. Upon excitation with near-IR laser line (785 nm), far away from the electronic absorption band (Alvarez-Puebla, Contreras-Caceres et al. 2009), NBA supported onto the metal core will produce a normal SERS signal. On the other hand, if NBA is excited with a red laser (633 nm), perfectly matching the absorption band, either SERRS or SEF will be produced, depending on the distance to the metal surface. Under these conditions, as the analyte is close enough to the gold, fluorescence can be quenched; however, if the molecule is not as close, it will feel the electromagnetic field enhancement generated by metallic core. Despite SERS and SERRS spectra overlap band to band, their relative intensities are not similar; this is because to the SERRS signal is not only influenced by the surface selection rules (Moskovits and Suh 1984; Moskovits 1985), but also by the resonance effects (Long 2002). Fig. 7 illustrates both SERS and SERRS spectra for NBA molecules immersed into the nanoparticle dispersion; spectra are characterized by the ring stretching (1643, 1492, 1440, 1387, 1351, and 1325 cm$^{-1}$), CH bending (1258, 1185 cm$^{-1}$), and the in-plane CCC and NCC (673 cm$^{-1}$), CCC and CNC (595 cm$^{-1}$), and CCC (499 cm$^{-1}$) deformations (Lu, Mei et al. 2006). The bands at 673 and 595 cm$^{-1}$ are significantly more enhanced for SERRS than for SERS, indicating that they correspond to the chromophore (phenoxazine), whereas the electronic resonance tends to enhance scattering bands from chemical groups absorbing the excitation laser line. In addition, SEF spectra is very similar to those obtained for standard fluorescence, with maximum emission at 668 nm (Aslan, Lakowicz et al. 2005). Regarding the temperature influence, as the analyte NBA is added to the particle dispersion at 4$^o$C and excited with NIR laser line (785 5nm), SERS intensity is very weak (Fig. 7a). Unlike the results obtained for 1NAT, where the intensity remains constant with temperature, here the intensity notably increases as shell collapses at 60$^o$C and diminishes again after cooling back to 4$^o$C . When the same sample is excited with a laser operating at 633 nm, the spectrum of the initial, swollen sample shows an intense fluorescence of about 16-fold the normal fluorescence. Instead, as temperature rises to 60$^o$C (collapsed shell), fluorescence quenches and SERRS spectrum is recovered. After subsequent cooling to 4$^o$C, less-intense SERRS spectrum can still be identified on top the strong SEF background.

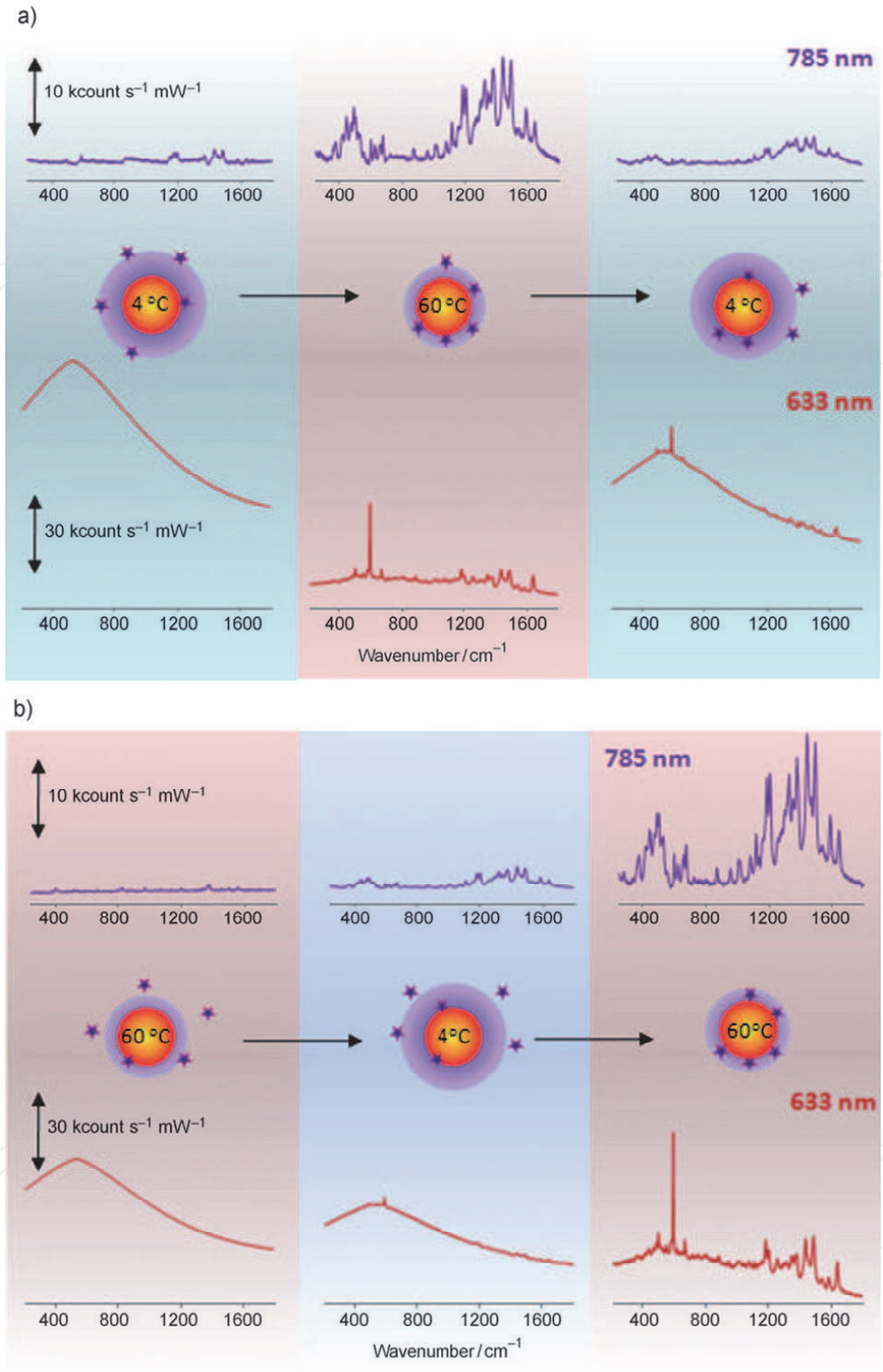


Fig. 7. SERS and SEF/SERRS spectra of Nile Blue A as a function of temperature. The excitation wavelength is $\lambda_{ex}$=785 nm (blue trace) and $\lambda_{ex}$=633 nm (red trace) for SERS and SEF/SERRS, respectively. Two different cooling-heating cycles are tested: (a) from 4 to 60 to 4°C; and (b) from 60 to 4 to 60°C. The acquisition time is 2s. Reprinted with permission from (Contreras-Caceres, Sanchez-Iglesias et al. 2008), Copyright (2008) by Wiley-VSC Verlag GmbH & Co. KGaA.

The disagreement between results concerning NBA and 1NAT molecules (for the temperature cycle 4-60-4 $^{o}$C) is attributed to the different affinity between amine and thiol groups for gold; the retention of NBA molecules on gold surface is less stable than for 1NAT, which causes partial release of NBA, thereby contributing to SERS and SERRS weakening (concomitantly to SFE enhancement). Interestingly, for the inverse cycle (60-4-60 $^{o}$C) (Fig. 7b), strong SEF intensity is recorded at 60$^{o}$C, which turns upon shell swelling into a weak SERRS signal (4$^{o}$C) and then to an intense SERRS spectra after final heating up to 60$^{o}$C. These results are interpreted by considering the shell swelling properties as well as the affinity of the analyte to gold. Due to the low affinity of NBA, even for the particle swollen state, the analyte does not significantly absorb onto gold cores (weak SERS signal at 4$^{o}$C), but it can be entrapped within the polymer network (strong SEF that completely screens the SERRS signal). When temperature raises up to 60$^{o}$C, the shells collapse and NBA molecules are entrapped closer to the core, as indicates the notable increase of SERS and SERRS, while SEF signal is quenched. For the second cycle (60-4-60$^{o}$C), a similar behaviour is found; initially, as particles collapse, only SEF is recorded. Upon particle swelling and subsequent collapse, NBA molecules are retained in close contact to the gold core surfaces. SERS signal then recovers. The entrapping mechanism is closely related to the hydrophilic-hydrophobic transition of pNIPAM microgels and to the microcapillarity effect occurring during particle collapse (Guerrini, Garcia-Ramos et al. 2006; Guerrini, Garcia-Ramos et al. 2008).

#### 4.2.2. 1-naphthol

SERS enhancement for Au-pNIPAM nanocomposite is finally tested for 1-napthol; this molecule does not easily adsorb onto conventional gold or silver surfaces, so its SERS analysis has remain elusive to date. Fig.8 illustrates SERS spectrum, recorded for the first time for 1-naphthol; it is characterized by CH bending (1447 cm$^{-1}$), ring stretching (1390 cm$^{-1}$), CCC in-plane deformation (842 cm$^{-1}$), CH out-of-plane deformation, ring breathing (716 cm$^{-1}$), ring deformation (655 and 584 cm$^{-1}$) and, ring twisting (477 cm$^{-1}$), in close agreement with the Raman assignment previously reported (Lakshminarayan and Knee 1990). SERS signal is properly identified after shell collapse, from 4$^{o}$C to 60$^{o}$C; the analyte is first retained within the swollen polymer networks, at 4$^{o}$C and then, brought into contact with the gold surfaces upon shells collapse. After subsequent cooling, the polymer shells swell again and 1-napthol molecules release the metal surface, resulting in a dramatic loss of SERS signal. The low affinity of hydroxyl groups of the 1-napthol to gold surfaces is clearly shown in the reversibility of the SERS signal along the swell-collapse cycles.

## 5. Improved SERS detection via bimetallic sensors

In the previous section, we have shown the ability of Au@pNIPAM nanoparticles for entrapping and detecting analytes by means of SERS. Nevertheless, the use of hybrid particles with small cores and the impossibility of those materials to form hot spots due to the physical barrier imposed by the polymer, limits the enhancement and imposes a detection threshold. To overcome this limitation, hybrid materials with different compositions and morphologies are employed. The first alternative involves controlled growth of silver shells onto the gold cores, since it is well known that silver is much more efficient plasmonic material (Zhao, Pinchuk et al. 2008). The second one refers to morphology changes towards rod-shaped cores, with near field concentration areas at the

rods edges, (Vesseur, de Waele et al. 2007; Cai, Sainidou et al. 2009). In addition, the molecular affinity of the pNIPAM shell and analyte can be improved by tuning the polymer charge.

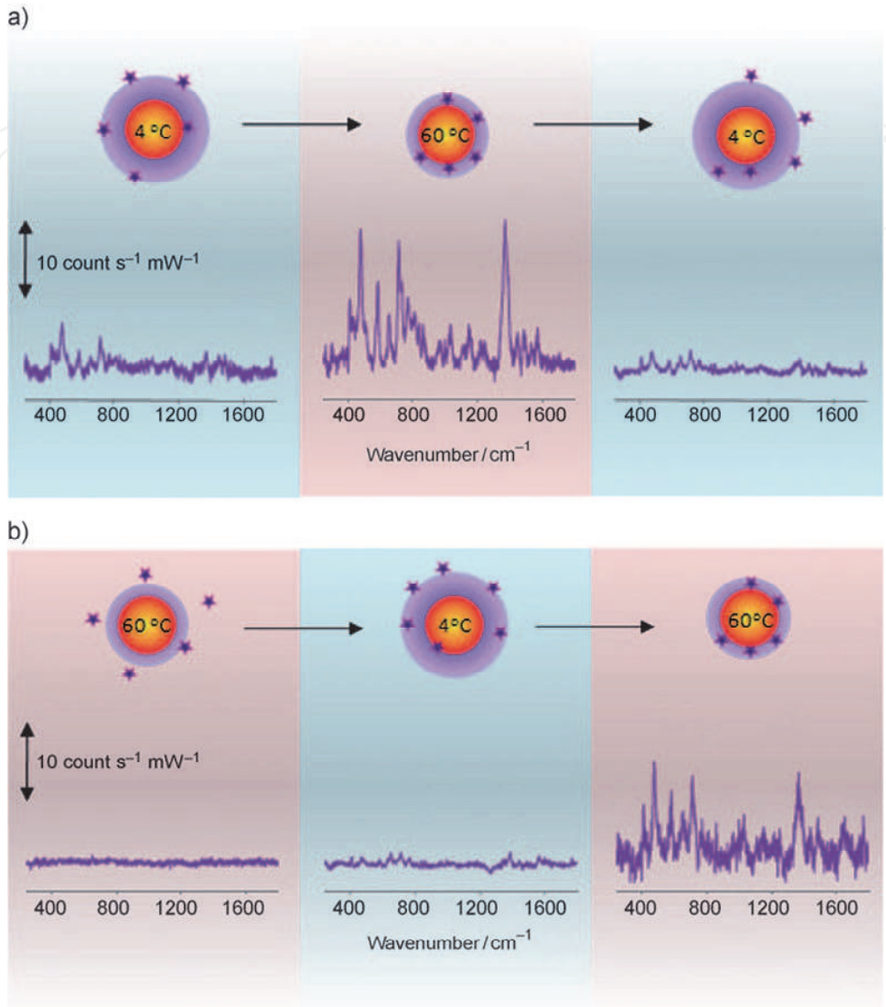


Fig. 8. Variation of SERS intensities of 1-napthol as a function of temperature for two different cooling-heating cycles: (a) from 4 to 60 to 4ºC; and (b) from 60 to 4 to 60ºC. The excitation wavelength is $\lambda_{ex}$=785 nm and the acquisition time 2s. Reprinted with permission from (Contreras-Caceres, Sanchez-Iglesias et al. 2008), Copyright (2008) by Wiley-VSC Verlag GmbH & Co. KGaA.

SERS detection is checked for a couple of analytes, 1-naphthalenethiol and 2-naphthoic (2-NA), using the whole set of hybrid particles prepared in section 3. Experiments are performed with a Renishaw Invia system, equipped with a Peltier charge-coupled device (CCD) detector and a Leica confocal microscope. Spectra are collected in Renishaw extended mode with accumulation times of 10 s using a macrosampling 90º objective adaptor. Samples are prepared by mixing 15 µL of analyte, previously dissolved either in ethanol (for 1-NAT) or aqueous alkaline solution with pH=13 (for 2-NA) at a concentration of $10^{-3}$ M, to

1.5 mL of the nanoparticle dispersion tested in each case. The mixtures are thermostatizated for 1 h before SERS recording.

### 5.1. Detection of 1-naphthalenethiol

SERS efficiency for gold and gold-silver nanoparticles coated with pNIPAM is first shown by using 1-naphthalenethiol. The spectra for 1NAT were already recorded in the presence of core-shell gold-pNIPAM particles, as we described in section 4.1. The excitation is now performed at three different lasers lines (inset on Figure 9), to make possible coupling of the respective surface plasmon modes. The intensity of the ring stretching peak (1368 $cm^{-1}$), at three wavelengths, is compared for all nanocomposites. All systems provide sufficient signal enhancement to allow identification of the analyte, which support the same mechanism proposed for spherical Au-pNIPAM particles irrespective of the core morphology and composition. 1NAT molecules reach the metallic cores by diffusion across the shells and bind onto the surfaces through thiol groups. Nevertheless, it appears substantial differences on signal enhancement; remarkably, for both spheres and rods, SERS intensity is found to increase with core size, although this improvement difference is moderate compared to the signal enhancement coming from the presence of silver. In addition, silver coatings induce spectral changes that lead us to use the green laser line (532 nm) to excite the LSPR; this wavelength is however very inefficient for pure gold particles due to damping effect

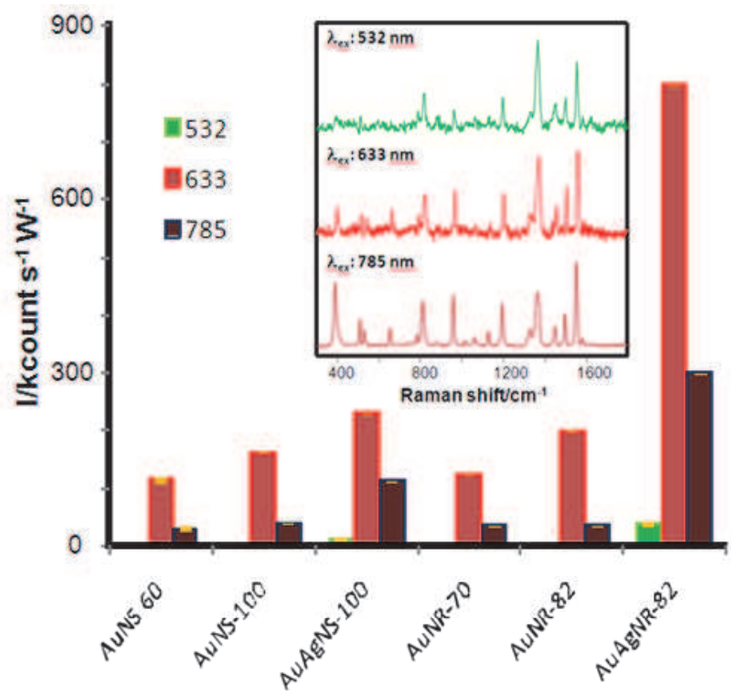


Fig. 9. Comparison of the Raman intensity corresponding to the ring stretching peak (1368 $cm^{-1}$) of 1NAT in different hybrid nanoparticle dispersions, acquired upon excitation with 532, 633 and 785 nm laser lines. The intensity is normalized with particle concentration in each case. The inset shows the SERS spectra of 1NAT in Au-pNIPAM suspension, recorded also at three different laser lines. Reprinted with permission from (Contreras-Caceres, Pastoriza-Santos et al.), Copyright (2010) by Wiley-VSC Verlag GmbH & Co. KGaA.

provoked by interband transitions. Even more interesting it is the large enhancement caused by the core morphology, with the intensity increasing as the spherical core transforms into rod. Change are particularly noticeable for gold-silver bimetallic nanorods since silver not only improves the optical efficiency, but also blue-shifts the longitudinal surface plasmon resonance, leading to stronger electric field concentration at the ends of the rods (Vesseur, de Waele et al. 2007; Cai, Sainidou et al. 2009). Thereby, both effects contribute to substantial increase of the SERS intensity upon excitation with red laser (633 nm).

### 5.2 Detection of 2-naphthoic acid

Improved SERS detection with bimetallic core nanoparticles is also shown using ionic analytes; 2-naphthoic acid (2NA). This analyte can be electrostatically entrapped by the polymer mesh in contrast to 1NAT, which chemically binds onto the metal cores through thiol groups. To this end, the analyte is first dissolved in pH=13 alkaline solution and subsequently added to dispersions with different nanoparticles, reaching a final pH=11. At that pH value, 2NA is completely ionized, bearing negative charge; as a result, it refuses to adsorb on standard citrate-stabilized silver particles due to their negative nature. Low Raman signal is then recorded in the presence of citrate-stabilized silver particles (Figure 10, up). Remarkably, Raman signal from NA is greatly enhanced when the analyte spectrum is recorded in the presence of core-shell hybrid particles (Figure 10, down). The well-defined spectra is characterized by the ring stretching at 1632 and 1388 $cm^{-1}$, CH bending at 1468 $cm^{-1}$, ring breathing at 1018 $cm^{-1}$, and CH deformation at 770 $cm^{-1}$ (Alvarez-Puebla and Aroca 2009). The presence of pNIPAM shells is responsible for the signal enhancement; since a

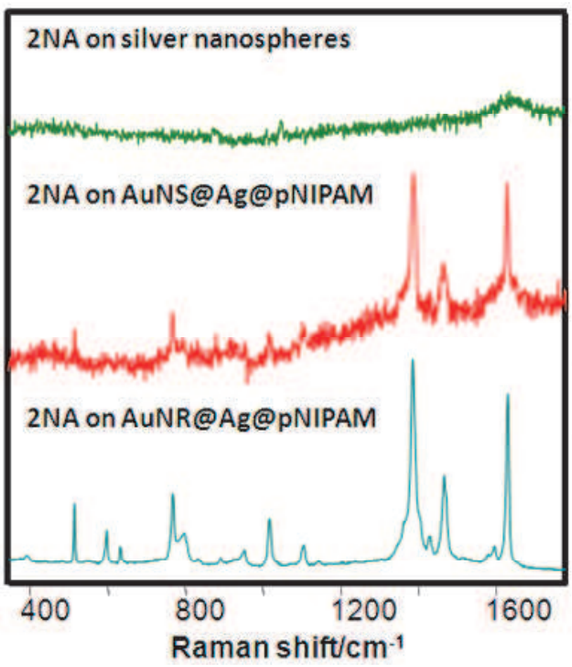


Fig. 10. SERS spectra of 2-naphtoic acid dissolved in an alkaline suspension of the different hybrid nanoparticles, acquired upon excitation with 532 nm laser line. Reprinted with permission from (Contreras-Caceres, Pastoriza-Santos et al.), Copyright (2010) by Wiley-VSC Verlag GmbH & Co. KGaA.

cationic initiator (AAPH) is used during polymerization, it displays a positive surface charge (+25mV), which is also present across the whole polymer network. Positive-charged shells can absorb 2NA anions by electrostatic interaction, then giving rise to significant SERS intensities. Although SERS enhancement is excellent for composites containing Au@Ag spherical cores, the signal is substantially larger for rod-shaped cores, thus confirming that the synergy between composition (silver) and morphology (rods) leads to much efficient SERS detection.

## 6. Conclusion

In this review we report the design, characterization and application of an advanced optical platform based on gold and gold-silver particles coated with polymeric pNIPAM shells. It allows ultra-sensitive analysis for a wide variety of analytes through Surface-enhanced Raman Spectroscopy. The composite particles combine optical amplification coming from metallic nanoparticles with singular thermoresponsive swelling features pNIPAM gels. Interestingly, the shell leads to entrap. The last one entraps physically analyte molecules and gets them close enough to the core surface, where signal enhancement is maximum. In addition, the shell can absorb charged molecules due to the presence of ionic groups anchored on the network, thus generalizing the use of these systems for SERS sensing. SERS enhancement is checked for different nanocomposite particles, paying special attention to the role of core geometry and metal composition. As expected, bimetallic gold-silver cores provide great SERS signal, especially intense for nanorod morphology.

## 7. Acknowledgement

Financial support from Spanish Ministerio de Ciencia e Innovación (Project MAT2010-17858), Andalucian Excellence Projects (FQM-02353 and FQM-230-2010), FEDER program and EU-COST Action D43 are acknowledged. The authors thank the great contribution of Prof. Luís Liz-Marzán, Dr. Ramón Álvarez-Puebla and Dr. Jorge Pérez-Juste to the content of this review.

## 8. References

Alvarez-Puebla, R. A., E. Arceo, et al. (2005). "Role of nanoparticle surface charge in surface-enhanced Raman scattering." Journal of Physical Chemistry B 109(9): 3787-3792.

Alvarez-Puebla, R. A. and R. F. Aroca (2009). "Synthesis of Silver Nanoparticles with Controllable Surface Charge and Their Application to Surface-Enhanced Raman Scattering." Analytical Chemistry 81(6): 2280-2285.

Alvarez-Puebla, R. A., R. Contreras-Caceres, et al. (2009). "Au@pNIPAM Colloids as Molecular Traps for Surface-Enhanced, Spectroscopic, Ultra-Sensitive Analysis." Angewandte Chemie-International Edition 48(1): 138-143.

Alvarez-Puebla, R. A., D. S. Dos Santos, et al. (2004). "Surface-enhanced Raman scattering for ultrasensitive chemical analysis of 1 and 2-naphthalenethiols." Analyst 129(12): 1251-1256.

Alvarez-Puebla, R. A., D. S. Dos Santos, et al. (2007). "SERS detection of environmental pollutants in humic acid-gold nanoparticle composite materials." Analyst 132: 1210-1214.

Aroca, R. F., R. A. Alvarez-Puebla, et al. (2005). "Surface-enhanced Raman scattering on colloidal nanostructures." Advances in Colloid and Interface Science 116(1-3): 45-61.

Aslan, K., J. R. Lakowicz, et al. (2005). "Metal-enhanced fluorescence using anisotropic silver nanostructures: critical progress to date." Analytical and Bioanalytical Chemistry 382(4): 926-933.

Aslan, K., M. Wu, et al. (2007). "Fluorescent core-shell Ag@SiO2 nanocomposites for metal-enhanced fluorescence and single nanoparticle sensing platforms." Journal of the American Chemical Society 129(6): 1524-1525.

Bao, L. L., S. M. Mahurin, et al. (2003). "Study of silver films over silica beads as a surface-enhanced Raman scattering (SERS) substrate for detection of benzoic acid." Journal of Raman Spectroscopy 34(5): 394-398.

Barnes, W. L., A. Dereux, et al. (2003). "Surface plasmon subwavelength optics." Nature 424(6950): 824-830.

Bell, S. E. J. and N. M. S. Sirimuthu (2008). "Quantitative surface-enhanced Raman spectroscopy." Chemical Society Reviews 37(5): 1012-1024.

Bohren, C. F. and D. R. Huffman (1983). Absorption and Scattering of Light by Small Particles. New York, Wiley.

Braeckmans, K., S. C. De Smedt, et al. (2002). "Encoding microcarriers: Present and future technologies." Nature Reviews Drug Discovery 1(6): 447-456.

Brown, L. O. and S. K. Doorn (2008). "Optimization of the preparation of glass-coated, dye-tagged metal nanoparticles as SERS substrates." Langmuir 24(5): 2178-2185.

Cai, W., R. Sainidou, et al. (2009). "Efficient Generation of Propagating Plasmons by Electron Beams." Nano Letters 9(3): 1176-1181.

Campion, A. and P. Kambhampati (1998). "Surface-enhanced Raman scattering." Chemical Society Reviews 27(4): 241-250.

Contreras-Caceres, R., J. Pacifico, et al. (2009). "Au@pNIPAM Thermosensitive Nanostructures: Control over Shell Cross-linking, Overall Dimensions, and Core Growth." Advanced Functional Materials 19(19): 3070-3076.

Contreras-Caceres, R., I. Pastoriza-Santos, et al. "Growing Au/Ag Nanoparticles within Microgel Colloids for Improved Surface-Enhanced Raman Scattering Detection." Chemistry-a European Journal 16(31): 9462-9467.

Contreras-Caceres, R., A. Sanchez-Iglesias, et al. (2008). "Encapsulation and growth of gold nanoparticles in thermoresponsive microgels." Advanced Materials 20(9): 1666-1670.

Creighton, J. A., C. G. Blatchford, et al. (1979). "Plasma resonance enhancement of raman-scattering by pyridine adsorbed on silver or gold sol particles of size comparable to the excitation wavelength." Journal of the Chemical Society-Faraday Transactions Ii 75: 790-798.

Chen, H. J., X. S. Kou, et al. (2008). "Shape- and size-dependent refractive index sensitivity of gold nanoparticles." Langmuir 24(10): 5233-5237.

Cho, E. C., P. H. C. Camargo, et al. "Synthesis and Characterization of Noble-Metal Nanostructures Containing Gold Nanorods in the Center." Advanced Materials 22(6): 744-748.

Fleischm.M, P. J. Hendra, et al. (1974). "Raman-Spectra of Pyridine Adsorbed at a Silver Electrode." Chemical Physics Letters 26(2): 163-166.

Gorelikov, I., L. M. Field, et al. (2004). "Hybrid microgels photoresponsive in the near-infrared spectral range." Journal of the American Chemical Society 126(49): 15938-15939.

Grancharov, K., H. Engelberg, et al. (2001). "Inhibition of UDP-glucuronosyltransferases in rat liver microsomes by natural mutagens and carcinogens." Archives of Toxicology 75(10): 609-612.

Guerrini, L., J. V. Garcia-Ramos, et al. (2006). "Functionalization of Ag nanoparticles with dithiocarbamate calix[4]arene as an effective supramolecular host for the surface-enhanced Raman scattering detection of polycyclic aromatic hydrocarbons." Langmuir 22(26): 10924-10926.

Guerrini, L., J. V. Garcia-Ramos, et al. (2008). "Building highly selective hot spots in Ag nanoparticles using bifunctional viologens: Application to the SERS detection of PAHs." Journal of Physical Chemistry C 112(20): 7527-7530.

Hansen, A. M., O. Omland, et al. (1994). "Correlation between work process-related exposure to polycyclic aromatic-hydrocarbons and urinary levels of alpha-naphthol, beta-naphthylamine and 1-hydroxypyrene in iron foundry workers." International Archives of Occupational and Environmental Health 65(6): 385-394.

Homola, J. (2008). "Surface plasmon resonance sensors for detection of chemical and biological species." Chemical Reviews 108(2): 462-493.

Hong, P. P., F. J. Boerio, et al. (1993). "Surface segregation in blends of polystyrene and deuterated polystyrene." Macromolecules 26(6): 1460-1464.

Hutter, E. and J. H. Fendler (2004). "Exploitation of localized surface plasmon resonance." Advanced Materials 16(19): 1685-1706.

Jain, P. K. and M. A. El-Sayed (2007). "Universal scaling of plasmon coupling in metal nanostructures: Extension from particle pairs to nanoshells." Nano Letters 7(9): 2854-2858.

Jain, P. K., X. H. Huang, et al. (2008). "Noble Metals on the Nanoscale: Optical and Photothermal Properties and Some Applications in Imaging, Sensing, Biology, and Medicine." Accounts of Chemical Research 41(12): 1578-1586.

Jana, N. R., L. Gearheart, et al. (2001). "Seeding growth for size control of 5-40 nm diameter gold nanoparticles." Langmuir 17(22): 6782-6786.

Johnson, P. B. and R. W. Christy (1972). "Optical-Constants of Noble-Metals." Physical Review B 6(12): 4370-4379.

Karg, M., I. Pastoriza-Santos, et al. (2006). "A versatile approach for the preparation of thermosensitive PNIPAM core-shell microgels with nanoparticle cores." Chemphyschem 7(11): 2298-2301.

Karg, M., I. Pastoriza-Santos, et al. (2007). "Nanorod-coated PNIPAM microgels: Thermoresponsive optical properties." Small 3: 1222-1229.

Kelly, K. L., E. Coronado, et al. (2003). "The optical properties of metal nanoparticles: The influence of size, shape, and dielectric environment." Journal of Physical Chemistry B 107(3): 668-677.

Kim, J. H. and T. R. Lee (2004). "Thermo- and pH-responsive hydrogel-coated gold nanoparticles." Chemistry of Materials 16(19): 3647-3651.

Kneipp, J., H. Kneipp, et al. (2006). "In vivo molecular probing of cellular compartments with gold nanoparticles and nanoaggregates." Nano Letters 6(10): 2225-2231.

Kneipp, K., H. Kneipp, et al. (1999). "Ultrasensitive chemical analysis by Raman spectroscopy." Chemical Reviews 99(10): 2957-2975.

Kneipp, K., Y. Wang, et al. (1997). "Single molecule detection using surface-enhanced Raman scattering (SERS)." Physical Review Letters 78(9): 1667-1670.

Kozumbo, W. J., S. Agarwal, et al. (1992). "Breakage and binding of dna by reaction-products of hypochlorous acid with aniline, 1-naphthylamine, or 1-naphthol." Toxicology and Applied Pharmacology 115(1): 107-115.

Kratz, K., T. Hellweg, et al. (2001). "Structural changes in PNIPAM microgel particles as seen by SANS, DLS, and EM techniques." Polymer 42(15): 6631-6639.

Lakshminarayan, C. and J. L. Knee (1990). "Spectroscopy and dynamics of the s1 state of jet-cooled 1-naphthol." Journal of Physical Chemistry 94(6): 2637-2643.

Lee, J., A. O. Govorov, et al. (2005). "Nanoparticle assemblies with molecular springs: A nanoscale thermometer." Angewandte Chemie-International Edition 44(45): 7439-7442.

Link, S. and M. A. El-Sayed (1999). "Spectral properties and relaxation dynamics of surface plasmon electronic oscillations in gold and silver nanodots and nanorods." Journal of Physical Chemistry B 103(40): 8410-8426.

Liu, M. Z. and P. Guyot-Sionnest (2005). "Mechanism of silver(I)-assisted growth of gold nanorods and bipyramids." Journal of Physical Chemistry B 109(47): 22192-22200.

Lombardi, J. R., R. L. Birke, et al. (1986). "Charge-Transfer Theory of Surface Enhanced Raman-Spectroscopy - Herzberg-Teller Contributions." Journal of Chemical Physics 84(8): 4174-4180.

Long, D. A., Ed. (2002). The Raman Effect: A Unified Treatment of the Theory of Raman Scattering by Molecules. Chichester, Wiley.

Lu, Y., Y. Mei, et al. (2006). "Thermosensitive core-shell particles as carriers for Ag nanoparticles: Modulating the catalytic activity by a phase transition in networks." Angewandte Chemie-International Edition 45(5): 813-816.

McFarland, A. D., M. A. Young, et al. (2005). "Wavelength-scanned surface-enhanced Raman excitation spectroscopy." Journal of Physical Chemistry B 109(22): 11279-11285.

Moskovits, M. (1985). "Surface-enhanced spectroscopy." Reviews of Modern Physics 57(3): 783-826.

Moskovits, M. (2006). Surface-enhanced Raman spectroscopy: a brief perspective. Surface-Enhanced Raman Scattering: Physics and Applications. 103: 1-17.

Moskovits, M. and J. S. Suh (1984). "Surface selection-rules for surface-enhanced raman-spectroscopy - calculations and application to the surface-enhanced Raman-spectrum of phthalazine on silver." Journal of Physical Chemistry 88(23): 5526-5530.

Mulvaney, P. (1996). "Surface plasmon spectroscopy of nanosized metal particles." Langmuir 12(3): 788-800.

Murphy, C. J., T. K. San, et al. (2005). "Anisotropic metal nanoparticles: Synthesis, assembly, and optical applications." Journal of Physical Chemistry B 109(29): 13857-13870.

Nie, S. M. and S. R. Emery (1997). "Probing single molecules and single nanoparticles by surface-enhanced Raman scattering." Science 275(5303): 1102-1106.

Njoki, P. N., I. I. S. Lim, et al. (2007). "Size correlation of optical and spectroscopic properties for gold nanoparticles." Journal of Physical Chemistry C 111: 14664-14669.

Okamoto, S. and S. Hachisu (1977). "Ordered Structure in Monodisperse Gold Sol." Journal of Colloid and Interface Science 62(1): 172-181.

Oldenburg, S. J., R. D. Averitt, et al. (1998). "Nanoengineering of optical resonances." Chemical Physics Letters 288(2-4): 243-247.

Otto, A., I. Mrozek, et al. (1992). "Surface-Enhanced Raman-Scattering." Journal of Physics-Condensed Matter 4(5): 1143-1212.

Pearson, R. G. (1963). "Hard and soft acids and bases." Journal of the American Chemical Society 85(22): 3533-3539"

Pearson, R. G. (1966). "Acids and bases." Science 151(3707): 172-177.

Penn, S. G., L. He, et al. (2003). "Nanoparticles for bioanalysis." Current Opinion in Chemical Biology 7(5): 609-615.

Pillai, S., K. R. Catchpole, et al. (2007). "Surface plasmon enhanced silicon solar cells." Journal of Applied Physics 101(9): 93105-93112.

Porter, M. D., R. J. Lipert, et al. (2008). "SERS as a bioassay platform: fundamentals, design, and applications." Chemical Society Reviews 37(5): 1001-1011.

Qian, X. M. and S. M. Nie (2008). "Single-molecule and single-nanoparticle SERS: from fundamental mechanisms to biomedical applications." Chemical Society Reviews 37(5): 912-920.

Rodriguez-Fernandez, J., J. Perez-Juste, et al. (2006). "Seeded growth of submicron Au colloids with quadrupole plasmon resonance modes." Langmuir 22(16): 7007-7010.

Rodriguez-Gonzalez, B., A. Burrows, et al. (2005). "Multishell bimetallic AuAg nanoparticles: synthesis, structure and optical properties." Journal of Materials Chemistry 15(17): 1755-1759.

Sanchez-Iglesias, A., E. Carbo-Argibay, et al. "Rapid Epitaxial Growth of Ag on Au Nanoparticles: From Au Nanorods to Core-Shell Au@Ag Octahedrons." Chemistry-a European Journal 16(19): 5558-5563.

Sanchez-Iglesias, A., M. Grzelczak, et al. (2009). "Synthesis of Multifunctional Composite Microgels via In Situ Ni Growth on pNIPAM-Coated Au Nanoparticles." Acs Nano 3(10): 3184-3190.

Schatz, G. C. (1984). "Theoretical-Studies of Surface Enhanced Raman-Scattering." Accounts of Chemical Research 17(10): 370-376.

Schlucker, S. (2009). "SERS Microscopy: Nanoparticle Probes and Biomedical Applications." Chemphyschem 10(9-10): 1344-1354.

Sepulveda, B., P. C. Angelome, et al. (2009). "LSPR-based nanobiosensors." Nano Today 4(3): 244-251.

Sierra-Martin, B., Y. Choi, et al. (2005). "Microscopic signature of a microgel volume phase transition." Macromolecules 38(26): 10782-10787.

Smith, E. and G. Dent (2005 ). Modern Raman Spectroscopy: A Practical Approach., John Wiley and Sons.

Stevenson, C. L. and T. Vo-Dinh (1996). Modern Techniques in Raman Spectroscopy New York, Wiley.

Stiles, P. L., J. A. Dieringer, et al. (2008). "Surface-Enhanced Raman Spectroscopy." Annual Review of Analytical Chemistry 1: 601-626.

Sun, H., O. X. Shen, et al. (2008). "Carbaryl, 1-naphthol and 2-naphthol inhibit the beta-1 thyroid hormone receptor-mediated transcription in vitro." Toxicology 249(2-3): 238-242.

Tian, Z. Q., B. Ren, et al. (2002). "Surface-enhanced Raman scattering: From noble to transition metals and from rough surfaces to ordered nanostructures." Journal of Physical Chemistry B 106(37): 9463-9483.

Vesseur, E. J. R., R. de Waele, et al. (2007). "Direct observation of plasmonic modes in Au nanowires using high-resolution cathodoluminescence Spectroscopy." Nano Letters 7(9): 2843-2846.

Vesseur, E. J. R., R. de Waele, et al. (2007). "Direct observation of plasmonic modes in Au nanowires using high-resolution cathodoluminescence Spectroscopy." Nano Letters 7: 2843-2846.

Vo-Dinh, T. (1998). "Surface-enhanced Raman spectroscopy using metallic nanostructures." Trac-Trends in Analytical Chemistry 17(8-9): 557-582.

Wang, H., F. Tam, et al. (2005). "Cu nanoshells: Effects of interband transitions on the nanoparticle plasmon resonance." Journal of Physical Chemistry B 109(39): 18218-18222.

Watson, D. A., L. O. Brown, et al. (2008). "A flow cytometer for the measurement of Raman spectra." Cytometry Part A 73A(2): 119-128.

Willets, K. A. and R. P. Van Duyne (2007). "Localized surface plasmon resonance spectroscopy and sensing." Annual Review of Physical Chemistry 58: 267-297.

Xu, H. X., J. Aizpurua, et al. (2000). "Electromagnetic contributions to single-molecule sensitivity in surface-enhanced Raman scattering." Physical Review E 62(3): 4318-4324.

Yang, Z. S., Y. W. Lin, et al. (2005). "Impacts that pH and metal ion concentration have on the synthesis of bimetallic and trimetallic nanorods from gold seeds." Journal of Materials Chemistry 15(25): 2450-2454.

Yavuz, M. S., W. Y. Li, et al. (2009). "Facile Synthesis of Gold Icosahedra in an Aqueous Solution by Reacting HAuCl4 with N-Vinyl Pyrrolidone." Chemistry-a European Journal 15(47): 13181-13187.

Zayats, A. V., Smolyaninov, II, et al. (2005). "Nano-optics of surface plasmon polaritons." Physics Reports-Review Section of Physics Letters 408(3-4): 131-314.

Zha, L. S., Y. Zhang, et al. (2002). "Monodisperse temperature-sensitive microcontainers." Advanced Materials 14(15): 1090-1092.

Zhao, J., A. O. Pinchuk, et al. (2008). "Methods for Describing the Electromagnetic Properties of Silver and Gold Nanoparticles." Accounts of Chemical Research 41(12): 1710-1720.

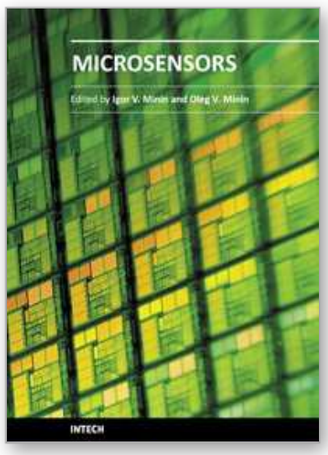


**Microsensors**

Edited by Prof. Igor Minin

ISBN 978-953-307-170-1

Hard cover, 294 pages

**Publisher** InTech

**Published online** 09, June, 2011

**Published in print edition** June, 2011

This book is planned to publish with an objective to provide a state-of-art reference book in the area of microsensors for engineers, scientists, applied physicists and post-graduate students. Also the aim of the book is the continuous and timely dissemination of new and innovative research and developments in microsensors. This reference book is a collection of 13 chapters characterized in 4 parts: magnetic sensors, chemical, optical microsensors and applications. This book provides an overview of resonant magnetic field microsensors based on MEMS, optical microsensors, the main design and fabrication problems of miniature sensors of physical, chemical and biochemical microsensors, chemical microsensors with ordered nanostructures, surface-enhanced Raman scattering microsensors based on hybrid nanoparticles, etc. Several interesting applications area are also discusses in the book like MEMS gyroscopes for consumer and industrial applications, microsensors for non invasive imaging in experimental biology, a heat flux microsensor for direct measurements in plasma surface interactions and so on.



INTECH
open science | open minds

**InTech Europe**
University Campus STeP Ri
Slavka Krautzeka 83/A
51000 Rijeka, Croatia
Phone: +385 (51) 770 447
Fax: +385 (51) 686 166
www.intechopen.com

**InTech China**
Unit 405, Office Block, Hotel Equatorial Shanghai
No.65, Yan An Road (West), Shanghai, 200040, China
中国上海市延安西路65号上海国际贵都大饭店办公楼405单元
Phone: +86-21-62489820
Fax: +86-21-62489821

IntechOpen